This is an open access article published under an ACS AuthorChoice License, which permits copying and redistribution of the article or any adaptations for non-commercial purposes.

ACS OMEGA

Article

Cite This: ACS Omega 2019, 4, 5829−5838

http://pubs.acs.org/journal/acsodf

# Synthesis of a 3,4-Disubstituted 1,8-Naphthalimide-Based DNA Intercalator for Direct Imaging of *Legionella pneumophila*

Hemant Sharma,[†,§] Jagpreet S. Sidhu,[‡] Walid M. Hassen,[†] Narinder Singh,*[,‡] and Jan J. Dubowski*[,†]

[†]Laboratory for Quantum Semiconductors and Photon-Based BioNanotechnology, Interdisciplinary Institute for Technological Innovation (3IT), CNRS UMI-3463, Department of Electrical and Computer Engineering, Université de Sherbrooke, Sherbrooke, Québec J1K 0A5, Canada

[‡]Department of Chemistry, Indian Institute of Technology Ropar, Rupnagar, Punjab 140001, India

Supporting Information

**ABSTRACT:** The development of organic molecules to target nucleic acid is an active area of research at the interface of chemistry and biochemistry, which involves DNA binding, nuclear imaging, and antitumor studies. These molecules bind with DNA through covalent interactions, electrostatic interactions, or intercalation. However, they are less permeable to membrane, and they have a significant cytotoxicity, which limits their application under in vivo conditions. In the present work, various mono- and disubstituted 1,8-naphthalimides-based derivatives (**S-12**, **S-13**, **S-15**, and **S-21**) have been synthesized and characterized through various spectroscopic techniques. Among these, 3-amino-4-bromo-1,8-naphthalimide (**S-15**) was found to have an attractive water solubility and act as a nuclear imaging agent. The spectroscopic absorption and emission data showed that **S-15** has a strong affinity for salmon sperm DNA with a binding constant of $6.61 \times 10^4$ $M^{-1}$, and the ratiometric fluorescence intensity ($I_{489}/I_{552}$) of **S-15** has a linear relationship in the 0−50 $\mu$M range of DNA concentrations. It intercalates with DNA through the hydrophobic planar naphthalimide core as confirmed through cyclic voltammetry, circular dichroism, $^1$H NMR titration, and thermal denaturation studies. Positively charged amine groups also participate in H-bonding with the bases and backbone of DNA. The **S-15** intercalator showed a large Stokes shift and photostability, which made it attractive for direct imaging of *Legionella pneumophila*, without the need for a prior membrane permeabilization.

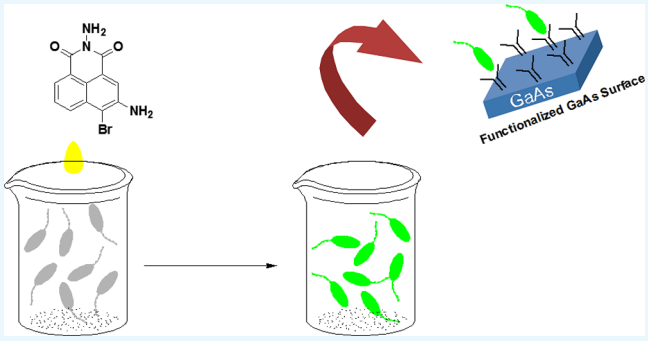


## INTRODUCTION

Recently, extensive work has been carried out to understand DNA organization, replication, and structure within the cell.[1,2] To achieve this goal, various dyes and metal complexes having imaging and therapeutic properties were designed and synthesized.[3−8] These dyes bind either covalently or non-covalently to DNA and behave as chemotherapeutic anticancer agents.[5,9,10] Unfortunately, poor membrane permeability, low water solubility, high toxicity, and photobleaching limit their application under in vivo conditions.[11] The traditional DNA dyes employed in cell imaging are categorized into two types:[12] (a) 4′,6-diamidino-2-phenylindole (DAPI), SYTO, and Hoechst stains, which are cell permeable and can be used for live cell imaging. Among these, DAPI and Hoechst stains require ultraviolet light for excitation, which may lead to DNA photodamage.[13] However, SYTO requires visible and near-infrared light as illumination, but low selectivity for nucleus hinders its application in cell imaging;[14] (b) thiazole orange ethidium bromide (EtBr, 3,8-diamino-5-ethyl-6-phenylphenanthridinium bromide) and propidium iodide dyes, which bind to DNA through intercalation, but they are poorly internalized by cell. Therefore, these dyes cannot be used for direct imaging of cell nucleus.

In addition to these points, conventional dyes have small Stokes shift (difference between emission and excitation wavelength) value usually less than 50 nm.[15−17] The large Stokes shift is a prerequisite to the sensitivity of fluorescence imaging because it minimizes the interaction between emission photons and excitation photons and gives high signal-to-noise ratio.[18−20] To address these issues, it is essential to carefully investigate the cell permeability, DNA binding ability, cytotoxicity, and photostability of DNA binding molecule. This information will act as a guide for the design of novel DNA binding molecule and imaging agent.

Recently, 1,8-naphthalimide derivatives have been extensively studied as cellular imaging agents and DNA intercalators.[21] They also exhibited an excellent antitumor activities under in vivo and in vitro conditions.[22−29] 4-Bromo-1,8-naphthalimide has been reported as an excellent inhibitor

Received: December 27, 2018
Accepted: March 14, 2019
Published: March 26, 2019


© 2019 American Chemical Society

DOI: 10.1021/acsomega.8b03638
ACS Omega 2019, 4, 5829−5838

**Scheme 1. Synthesis of S-12, S-13, and S-21**

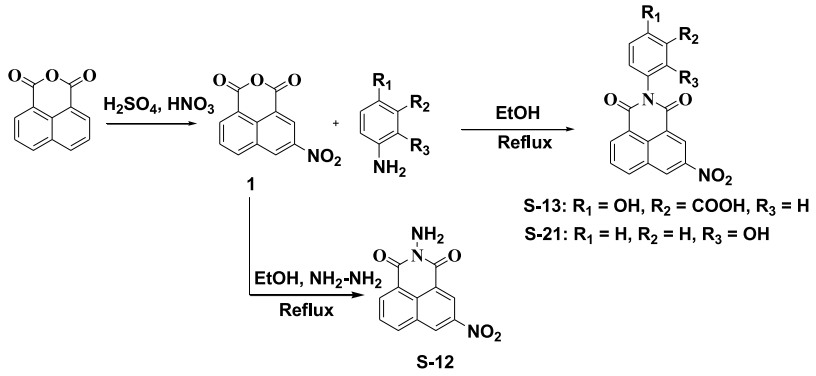


**Scheme 2. Synthesis of S-15**

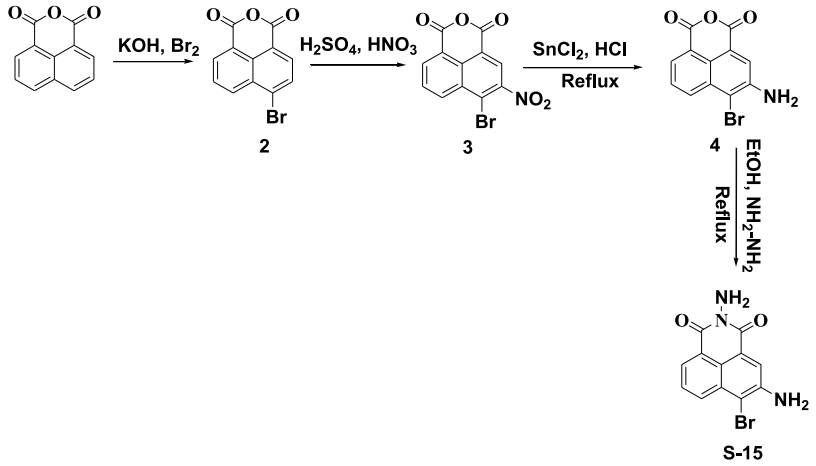


for enveloped viruses in blood and in blood products.[30−32] Other two main members of naphthalimide derivatives, amonafide (3-amino-1,8-naphthalimide) and mitonafide (3-nitro-1,8-naphthalimide), displayed a high antitumor activity ($IC_{50}$ 0.47 and 8.80 $\mu$M, respectively), and both have entered phase II clinical trials.[33,34] These compounds have high affinity for DNA and represent an important class of DNA-intercalator agent.[35] They induce DNA strand breaks and DNA-protein cross linking,[36,37] and inhibit nucleic acid synthesis[33] and interfering topoisomerase II activity.[38,39] From structure−activity relationship point of view, 3 and 4 positions substituted 1,8-naphthalimides have high activity, particularly 3-amino substituted.[33,34] To take this advantage, we are proposing 3-amino-4-bromo-1,8-naphthalimide as a DNA intercalator that is further utilized as an imaging agent for direct imaging of *Legionella pneumophila* without any pretreatment.

Photophysical properties of 1,8-naphthalimides can be tuned through substitution at proper place. The functionalization with amino group at the 3 and 4 positions of the naphthalimide ring shifts the absorbance and emission maximum to the visible region. These 3- and 4-amino-1,8-naphthalimide derivatives have high photostability and large Stokes shift in various aqueous and non-aqueous solvents.[40] Internal charge transfer (ICT) is attributed to these beneficial photophysical properties, which arises from electronic push−pull between the electron-withdrawing imide group and the electron-donating amino group.[40−48] Thus, these derivatives have been extensively employed in the development of chemosensors for metal ions, anions, and biomolecules.[40−42,49−51] Nonetheless, their role as an imaging agent under in vivo and in vitro conditions has not been sufficiently explored. We synthesized four 1,8-naphthalimide-based derivatives (**S-12**, **S-13**, **S-15**, and **S-21**) and found that **S-15** has an attractive water solubility, cell permeability, and high affinity to bind with DNA. The DNA-binding mechanism of **S-15** was studied using UV−visible spectroscopy, fluorescence spectroscopy, circular dichroism (CD) spectroscopy, $^1$H NMR titration, and cyclic voltammetry. We were not able to observe fluorescence from UV-exposed *L. pneumophila* treated with **S-15**. However, a clear fluorescence was observed for **S-15** treated with both live and heat killed *L. pneumophila* consistent with the expected reaction between **S-15** and bacterial DNA.

## RESULTS AND DISCUSSION

Schemes 1 and 2 illustrate the synthetic route for **S-12**, **S-13**, **S-15**, and **S-21**. Compounds **S-12**, **S-13**, and **S-21** were synthesized from a common precursor, 3-nitronaphthalimides (**1**), as shown in Scheme 1. The latter was synthesized through nitration of 1,8-naphthalimide. 3-Nitronaphthalimide with a particular amine refluxed and gave corresponding products **S-12**, **S-13**, and **S-21** with 65, 65, and 68% yields, respectively (Scheme 1).

Compound **S-15** was prepared through a series of steps, as illustrated in Scheme 2. First, 1,8-naphthalimide underwent bromination to give **2** with a 62% yield. It was followed by nitration with $H_2SO_4$ and $HNO_3$ and gave **3** with a 65% yield. Then, compound **3** underwent reduction with $SnCl_2$/HCl and gave compound **4**. This compound was further refluxed with



DOI: 10.1021/acsomega.8b03638
*ACS Omega* 2019, 4, 5829−5838

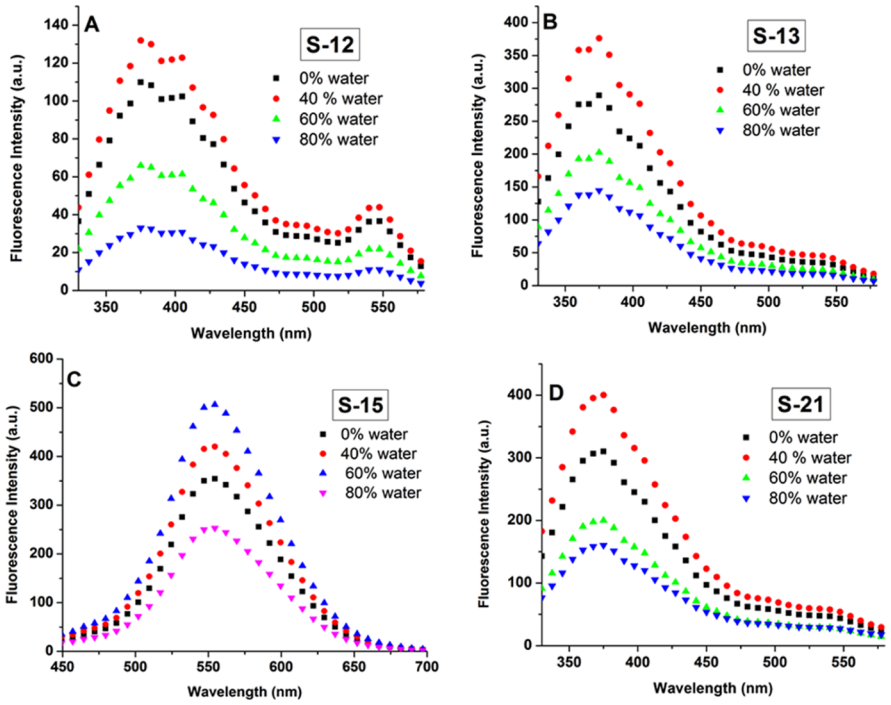


**Figure 1.** (A–D) Represent change in the emission spectra of **S-12** (10 $\mu$M), **S-13** (10 $\mu$M), **S-15** (10 $\mu$M), and **S-21** (10 $\mu$M) in different fractions of DMSO/$H_2O$.

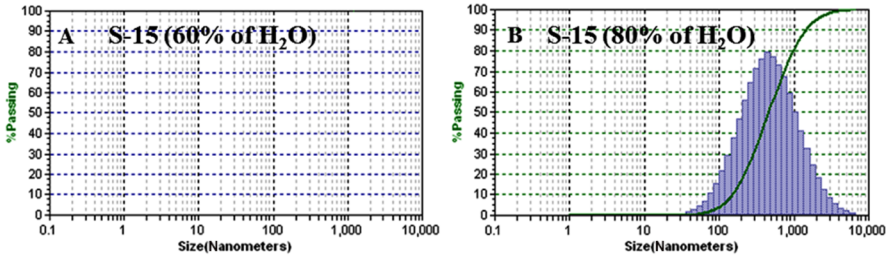


**Figure 2.** DLS spectra of **S-15** (10 $\mu$M) in (A) 60 and (B) 80% water fraction, respectively.

hydrazine hydrate in ethanol to obtain **S-15** with a 72% yield. All compounds thus obtained were characterized using $^1$H NMR, $^{13}$C NMR, and high-resolution mass spectrometry (HRMS) analytical techniques (see Supporting Information, Figures S1–S12).

The photophysical properties of the naphthalimide derivatives (**S-12**, **S-13**, **S-15**, and **S-21**) were recorded with UV–visible spectrophotometer and fluorescence. These compounds are known to be soluble in dimethyl sulfoxide (DMSO), but for biological applications, water solubility is essential. Therefore, we investigated the solubility of these derivatives in different fractions of water up to 80%. We found that up to 40% water fraction, a slight increase in the emission intensity takes place for all compounds, as illustrated in Figure 1. However, **S-12**, **S-13**, and **S-21** precipitated when the water content was increased to 60% (see Supporting Information, Figure S13) and their emission intensity decreased, as illustrated in Figure 1A,B,D, respectively. On further increase in water fraction (80%), more precipitation was observed in the cuvette, which led to decrease in the emission intensity of these compounds (Figure 1). In contrast, **S-15** showed an enhancement in the emission intensity at 552 nm up to 60% water fraction, as illustrated in Figure 1C, and no precipitate was noticed in the solution (see Supporting Information, Figure S13). The enhancement in emission intensity with increasing water fraction up to 60% is because of ICT.[52] However, further increase in water fraction led to quenching in the emission behavior of **S-15**. This quenching phenomenon may be the result of aggregation. To check the possibility of nanoaggregates formation, the dynamic light scattering (DLS) study was performed.

No aggregate formation was observed for **S-15** in 60% water fraction, as shown in Figure 2A. However, at 80% water fraction, aggregates were formed with a wide range of size, as shown in Figure 2B. DLS study indicated that aggregation-caused quenching is the responsible phenomenon for the decrease in emission intensity.[53,54] In addition, specific solvent–solute interactions may have also played a role in quenching of emission intensity at higher water fraction.[55] Thus, both these effects increase the non-radiative decay rates at 80% water fraction[56,57]

The water fraction study illustrates that only **S-15** has more water solubility compared to other derivatives. Consequently, 60% water fraction of **S-15** was selected to carry out the further experiments. The absorption and emission spectra of a 10 $\mu$M **S-15** in DMSO/$H_2O$ (4:6, v/v) solvent system are shown in Figure 3. An intense band at 342 nm is because of $\pi$–$\pi^*$ transitions,[21,52,58] and the broad visible band at 413 nm has



DOI: 10.1021/acsomega.8b03638
ACS Omega 2019, 4, 5829–5838

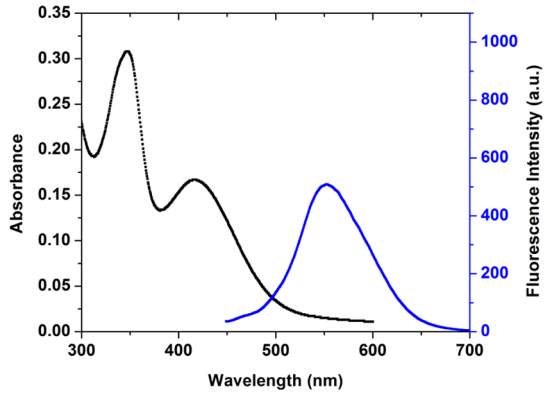


**Figure 3.** UV−visible absorption spectra and fluorescence spectra ($\lambda_{ex}$ = 430 nm; Ex. and Em. slit width 10 nm) of **S-15** (10 $\mu$M) in DMSO/$H_2O$ (4:6, v/v) solvent system.

been assigned to an ICT transition. It can be seen that **S-15** exhibits a large Stokes shift of ∼139 nm. Also, we found that **S-15** obeys the Beer−Lambert law at concentration of up to 80 $\mu$M in DMSO/$H_2O$ (4:6, v/v) solvent system, in agreement with literature data,[56] which suggests that only monomeric form of **S-15** exists under these conditions. To further investigate this effect, a set of solutions was prepared with **S-15** at 80, 100, and 150 $\mu$M concentrations. Our DLS experiments revealed that the aggregates form at concentration increased to 100 and 150 $\mu$M (see Supporting Information, Figure S14), consistent with the formation of $\pi-\pi$ stacking observed at higher concentrations of 1,8-naphthalimide derivatives.[56] Thus, in the present study, 10 and 30 $\mu$M solutions were used for DNA binding and imaging, respectively, that is, where no aggregates were expected to form. To investigate photostability, the emission intensity of **S-15** at 552 nm was recorded with time, and it can be seen that emission intensity did not decrease significantly even up to 6 h (see Supporting Information, Figure S15).

The DNA-binding ability of **S-15** was probed through monitoring absorption bands. The stock solution of salmon sperm-DNA (100 $\mu$M, pH 7.5) was prepared in tris-HCl buffer. The addition of DNA solution at 50 $\mu$M into **S-15** resulted in decreased absorbance at 342 and 413 nm, as shown in Figure 4A. The half-reciprocal plot shown in Figure 4B illustrates a dependence between the absorbance at 413 mm and the concentration of salmon sperm DNA. A continuous decrease in absorbance was observed followed by the saturation at high concentration of DNA (inset in Figure 4A). The decrease in absorbance was more than 50%. The intrinsic binding constant ($K$) was calculated using the following equation[59]

$$D/\Delta\varepsilon_{ap} = D/\Delta\varepsilon + 1/\Delta\varepsilon K \quad (1)$$

where $D$ is the concentration of DNA in base pairs, $\Delta\varepsilon_{ap} = [\varepsilon_a - \varepsilon_F]$, $\Delta\varepsilon = [\varepsilon_B - \varepsilon_F]$, $\varepsilon_a$ is apparent extinction coefficient ($A_{obsd}/$[**S-15**]), and $\varepsilon_B$ and $\varepsilon_F$ correspond to the apparent extinction coefficient of bound and free form of **S-15**, respectively. The $K$ value for a base pair was determined at 6.61 × $10^4$ $M^{-1}$. The large hypochromic shift is characteristic of intercalation,[12,58] and it indicates the close proximity of the **S-15** to the DNA bases.[59]

To study the excited-state interaction with DNA, fluorescence titration was performed. The stepwise addition of DNA into the solution of **S-15** resulted in a decreased emission at 552 nm and an enhanced emission at 489 nm, as shown in Figure 5A. The titration also showed a single isosbestic point at 514 nm for all DNA concentration (Figure 5A). It represents the existence of two types of distinct species. The ratiometric intensity ($I_{489}/I_{552}$) has a linear relationship with a range (0−50 $\mu$M) of DNA concentration (Figure 5B). The inset in Figure 5A shows a decrease in normalized intensity at 552 nm with the addition of DNA. This decrease in intensity may be aroused because of transfer of electron from the nucleotide to naphthalimide.[60] The binding constant was calculated using fluorescence data and was found to be 7.27 × $10^4$ $M^{-1}$ (see Supporting Information, Figure S16). The absorption and emission spectroscopy suggest that **S-15** binds with DNA through intercalation, with the planar naphthalimide core and positively charged amine groups responsible for this mode of interaction. In addition to emission and absorption spectroscopic evidences for intercalation mode of binding, $^1$H NMR titration of **S-15** was performed with DNA. The titration was performed through addition of different amounts of DNA (in $D_2O$) into the solution of **S-15**, and each addition was followed by $^1$H NMR measurement. Figure S17 represents the change in the aromatic proton region of **S-15** in different amounts of DNA. As the concentration of DNA increased, aromatic proton of **S-15** showed upfield shift along with signal broadening. This particular change corresponds to intercalative mode of binding.[61]

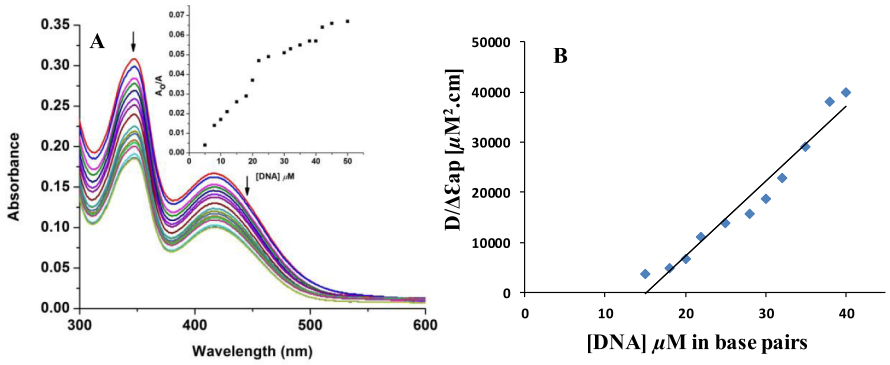


**Figure 4.** (A) UV−visible absorption spectra of **S-15** (10 $\mu$M) in the presence of increasing concentration of salmon sperm DNA (0−50 $\mu$M) in DMSO/$H_2O$ (4:6, v/v) solvent system; inset represents plot of $A_o/A$ vs concentration of DNA ($\mu$M); (B) half-reciprocal plot of **S-15** binding with salmon sperm DNA as calculated from the UV−visible absorption titration.



DOI: 10.1021/acsomega.8b03638
ACS Omega 2019, 4, 5829−5838

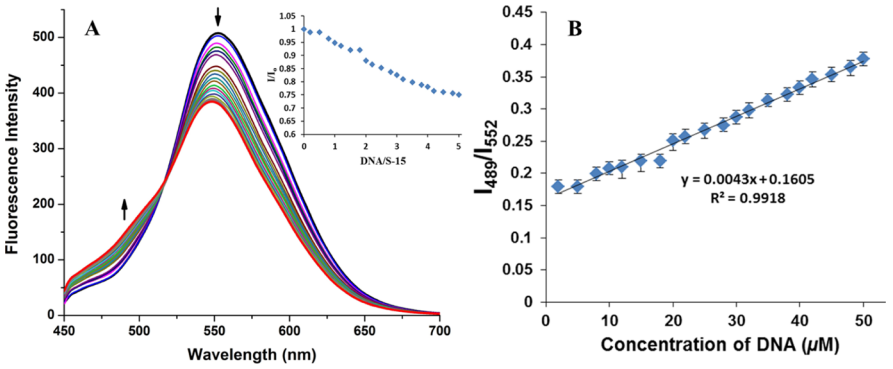


**Figure 5.** (A) Emission spectra of **S-15** (10 $\mu$M) in the presence of increasing concentration of salmon sperm DNA (0−50 $\mu$M) in DMSO/$H_2O$ (4:6, v/v) solvent system; inset represents plot of $I/I_o$ vs DNA/**S-15**; (B) ratiometric plot between $I_{489}/I_{552}$ and concentration of DNA ($\mu$M). $\lambda_{ex}$ = 430 nm; Ex. and Em. slit width 10 nm.

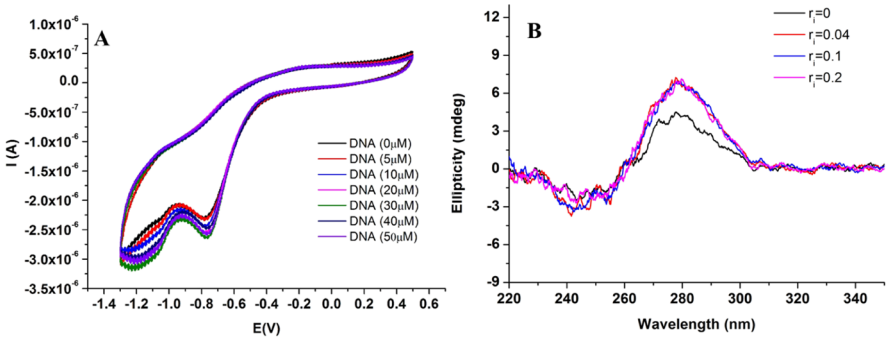


**Figure 6.** (A) Change in the CV profile of **S-15** (10 $\mu$M) in the presence of increasing concentration of DNA (0−50 $\mu$M) in DMSO/$H_2O$ (4:6, v/v) solvent system (scan rate 50 mV/s); (B) CD spectra of DNA (50 $\mu$M) at different ($r_i$ = **S-15**/DNA) ratios of **S-15** and DNA.

The binding mechanism was also confirmed through thermal denaturation study. Thermal denaturation studies are an attractive technique to investigate the interaction between small molecules and DNA. The binding of added molecules with DNA double helix results in increase in the melting temperature ($T_m$) (temperature at which DNA duplex is half denatured). As shown in Figure S18, absorbance at 260 nm of DNA (50 $\mu$M) was recorded in the presence and absence of **S-15** (10 $\mu$M) in the temperature range of 50−90 °C; $\Delta T_m$ was found to be 7.0 °C. The enhancement in $T_m$ indicated the intercalation between DNA and **S-15**.[62] The binding between **S-15** and DNA was further confirmed through the electrochemical method. The cyclic voltammogram (CV) of **S-15** (10 $\mu$M) has one irreversible peak at −0.77 V, and the addition of DNA to **S-15** solution did not produce any new peak (Figure 6A). However, the intensity of current was increased at −0.77 V, which indicates the interaction between **S-15** and DNA molecule.[62−64]

Furthermore, to investigate the conformational changes in DNA upon binding with **S-15**, CD spectra were recorded for different ratios of **S-15** and DNA. As indicated in Figure 6B, salmon sperm DNA has two bands in the CD spectra. The positive band at ∼275 nm indicates base stacking, and the negative band at ∼245 nm corresponds to helicity.[65] The addition of **S-15** enhanced the intensity of the band at 275 nm, and further addition of **S-15** did not cause any change in intensity. However, the band at 245 nm remained unchanged. The increase in intensity of base stacking band indicated the intercalation mode of binding between **S-15** and DNA.[66] These spectroscopic results indicated dual mode of interaction, electrostatic and intercalation, between **S-15** and DNA. The planar nature of hydrophobic core helps to probe to intercalate into the non-polar interior of the DNA helix.[21] Moreover, amine groups in **S-15** have a positive charge at physiological environment and are expected to facilitate H-bonding with the base and backbone of DNA.[23] To probe the interference from other biologically relevant analytes, fluorescence spectra of **S-15** were recorded with different biomolecules, and it was noticed that none of the analyte showed particular change in the emission profile of **S-15** (see Supporting Information, Figure S19).

The cellular uptake of **S-15** was investigated by exposing freshly cultivated *L. pneumophila* to a 30 $\mu$M solution of **S-15** in DMSO/$H_2O$ (4:6, v/v) solvent system. Bacteria were incubated with **S-15** for 1 h. This was followed by centrifugation for 30 min at 3000 rpm. The supernatant liquid was removed and the pellet was re-suspended in phosphate buffer saline (PBS). The dye-treated bacteria were immobilized specifically on the surface of a GaAs(001) chip functionalized with a self-assembled monolayer architecture comprising biotinylated-polyethylene-glycol (PEG) and hexadecane thiols/neutravidin/biotinylated-antibody, as illustrated in Figure 7. Previously, we employed a similar architecture for the immobilization of *Escherichia coli* on GaAs,[67] studying reaction of *E. coli* to antibiotics[68] and for rapid detection of *L. pneumophila*.[69]

Following the 1 h exposure of a biochip to a PBS solution with dye-treated bacteria at 4 × $10^5$ CFU/mL, it was washed with PBS three times to remove the loosely bound bacteria. The presence of bacteria on the surface of the biochip was analyzed using fluorescence microscopy (excitation and emission at 457−487 and 502−538 nm, respectively). As



DOI: 10.1021/acsomega.8b03638
*ACS Omega* 2019, 4, 5829−5838

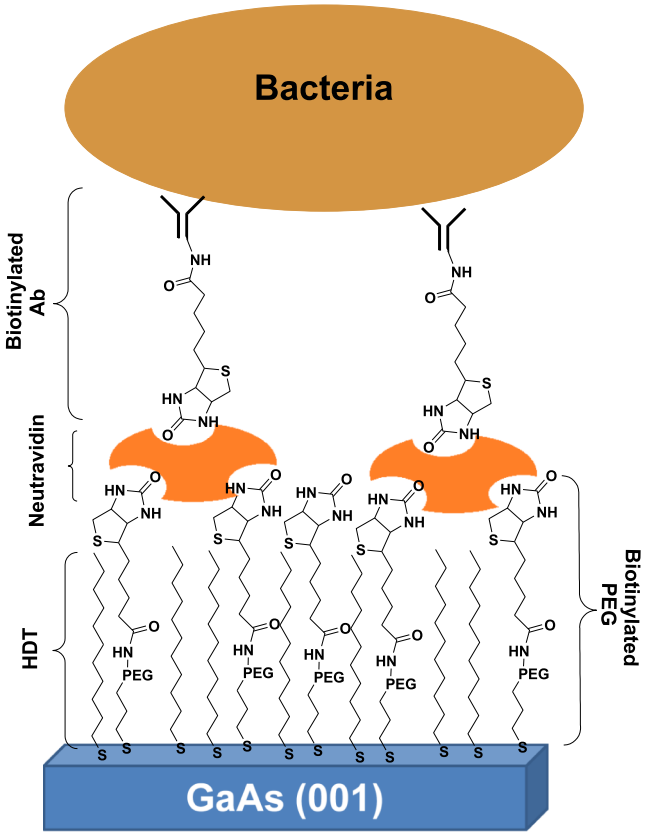


**Figure 7.** Pictorial view of a GaAs(001) biochip functionalized with a biotinylated-PEG/neutravidin/biotinylated antibody mixed with HDT architecture.

shown in Figure 8A, bacteria showed a significant fluorescence that remained stable over the extended period of time (~1 h). The analysis of surface coverage using ImageJ software revealed 25 ± 1.5 bacteria per $mm^2$ immobilized from a 4 × $10^5$ CFU/mL solution.

For comparison, two blank GaAs samples were prepared with the architecture, as presented in Figure 7. The first one was exposed to a 30 $\mu$M **S-15** solution free of bacteria, and the second to a bacteria solution at 4 × $10^5$ CFU/mL without the **S-15** dye. The inability to observe fluorescence in the blank samples (Figure 8B,C) irradiated under same conditions indicated that the **S-15** did not bind or precipitate on the surface of functionalized GaAs chip and fluorescence was observed only when the bacteria were treated with **S-15** prior to incubation with the functionalized GaAs chip. To investigate further, we employed UV-treated *L. pneumophila* that was obtained by exposing a bacterial solution to a mercury lamp emitting at ~254 nm for 5 min at room temperature, followed by incubation with **S-15** (30 $\mu$M). The absence of fluorescence in this case suggests that dye neither internalize nor bind on the surface of UV killed bacteria.

To understand the mode of penetration (active or passive) of **S-15** dye in the bacteria, the biofunctionalized biochip was exposed to *L. pneumophila* (4 × $10^5$ CFU/mL) heat killed at 90 °C for 20 min, followed by incubation with the dye (**S-15**). The heat-killed bacteria showed fluorescence (Figure 8D), which is possible only when the dye internalized into bacteria. The heating process significantly influences the cell permeability, and a long exposure to heat can result in cell leakage.[70] Therefore, the change in membrane permeability allows the dye to enter the bacteria that become fluorescent (Figure 8D). The analysis of surface coverage using ImageJ software revealed 17 ± 3 bacteria per $mm^2$ immobilized on the biochip surface. Thus, the above experiment indicated that fluorescence was observed only when the dye (**S-15**) was internalized into the bacteria.

The internalization of **S-15** was further investigated by confocal microscopy. The fully functionalized GaAs chip was incubated with 4 × $10^5$ CFU/mL of *L. pneumophila*. To stain the bacterial membrane, the biochip was exposed to rhodamine-red solution for 30 min. Next, the biochip was rinsed with 0.1× PBS three times to remove unbound rhodamine-red dye. The biochip was further incubated with the solution of **S-15** (30 $\mu$M) for 1 h. After washing with deionized (DI) water and drying, the biochip was placed in contact with a glass slide covered by an oil drop and incubated for 24 h. To image the rhodamine staining, the biochip was irradiated with excitation wavelength at 573 nm and emission was collected at 591 nm. The resulting image shown in Figure 8E indicated the staining of bacterial membrane, as evidenced by the red color emission, whereas no emission was observed from the core of bacteria. To observe the emission from **S-15** dye, the sample was excited at 450 nm and emission was observed at 530 nm. The continuous rod-shaped green emission was detected in this case, which indicates the internalization of **S-15** dye (Figure 8F). The merged image depicted the red emission observed from bacterial membrane and the green emission from inside of the bacteria (Figure 8G). Thus, as our spectroscopic studies

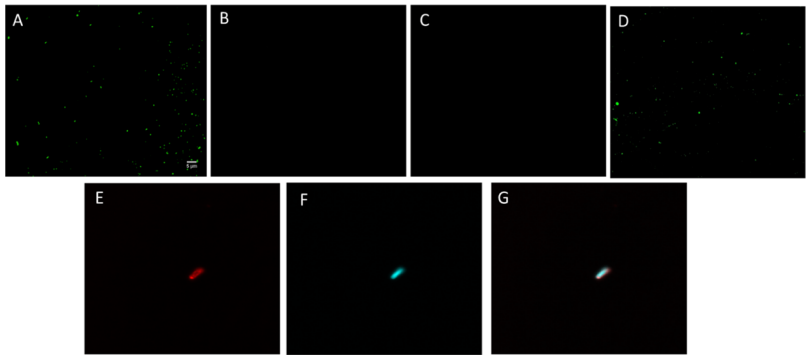


**Figure 8.** Fluorescence microscopy of biofunctionalized GaAs biochips exposed to: (A) live *L. pneumophila* treated with **S-15** (30 $\mu$M) scale 5 $\mu$m, (B) **S-15** only, (C) untreated *L. pneumophila*, (D) heat-killed *L. pneumophila* treated with **S-15** (30 $\mu$M), (E) confocal image of rhodamine-red stained *L. pneumophila*, (F) confocal image of **S-15** stained *L. pneumophila*, and (G) the merged image of (E,F).



DOI: 10.1021/acsomega.8b03638
*ACS Omega* 2019, 4, 5829−5838

show, **S-15** intercalates with DNA, which results in a significant change of its photophysical properties.

To investigate the effect of DMSO, optical images of *L. pneumophila* were recorded in 40% DMSO and compared with control in PBS solution. The image analysis showed that the size and shape of bacteria remained comparable in both environments (see Supporting Information, Figure S20). The cytotoxicity of **S-15** was also investigated toward the HeLa cell line in 3-(4,5-dimethylthiazol-2-yl)-2,5-diphenyltetrazolium bromide (MTT) assay. The dose-dependent studies (see Supporting Information, Figure S21) revealed that 90−97% cell remained viable following the exposure up to 50 $\mu$M concentration of **S-15**. This suggests that the synthesized intercalator could find applications in studying reactions involving DNA binding, nuclear imaging, and cancerous cell research.

## CONCLUSIONS

3-Amino-4-bromo-1,8-naphthalimide-based DNA intercalator (**S-15**) has been synthesized with two amine groups that provide positive charge at physiological pH. This positively charged moiety interacts with the bases and backbone of DNA (negatively charged) through the electrostatic interactions and H-bonding. Moreover, the planar hydrophobic naphthalimide ring of **S-15** intercalates with DNA. The complexation between DNA and **S-15** has been confirmed through UV−visible spectroscopy, emission spectroscopy, cyclic voltammetry, $^1$H NMR titration, and CD spectroscopy. The successive addition of DNA into the solution of **S-15** decreases the absorbance at 342 and 413 nm. However, the titration on fluorescence spectrophotometer showed a ratiometric change in the emission profile of **S-15**. CD spectra of salmon sperm DNA showed an increase in the ellipticity of the band at 275 nm in the presence of **S-15**, and $\Delta T_m$ was found increased by 7.0 °C compared to native DNA. Thus, these spectroscopic observations indicate intercalation as well as electrostatic interaction between **S-15** and DNA. Furthermore, the application of **S-15** has been demonstrated for successful staining and imaging of live *L. pneumophila* immobilized on the biofunctionalized surface of GaAs biochips.

## EXPERIMENTAL SECTION

**Materials and Methods.** All reagents were purchased from Sigma-Aldrich and used without further purification. $^1$H NMR and $^{13}$C NMR spectra were recorded in $CDCl_3$ and DMSO-$d_6$ with tetramethylsilane (TMS) as an internal reference. The NMR study was performed on a JNM-ECS400 (JEOL) instrument operating at 400 MHz for $^1$H NMR and 100 MHz for $^{13}$C NMR. The chemical shift ($\delta$) values were reported in parts per million relative to TMS, and splitting patterns were conceptualized as s (singlet), bs (broad singlet), d (doublet), dd (doublet of doublet), t (triplet), and m (multiplet). All absorption spectra were measured on a Shimadzu UV-2400 spectrophotometer, and emission spectra were recorded on a PerkinElmer LSS fluorescence spectrophotometer. To ensure the uniformity, solutions were shaken well prior to measurements. Electrochemical studies were recorded on a potentiostat−galvanostat BASi Epsilon. Each measurement was recorded in a single compartment cell equipped with a glass carbon working electrode, Pt wire counter electrode, and Ag/$AgNO_3$ reference electrode. The working electrode was cleaned through ultrasonication in ethanol and DI water. The size distribution of nanoaggregates was determined on a Metrohm Microtrac Ultra Nanotrac particle size analyzer (DLS). The DLS probe equipped with a laser diode allows to rapidly detect the size distribution of aggregates. The probe was carefully cleaned before measurements and dipped into the solution. CD spectra were measured on a JASCO, J-1500 CD spectrophotometer in the range between 220 and 400 nm. An Olympus IX71 fluorescence microscope was used to record the fluorescence images. The confocal images have been recorded using Olympus FV3000 microscope. The raw images were captured using a Plan Apochromat 63×/1.40 objective.

**Synthesis of S-12.** Compound **1** was synthesized according to the procedure reported in the literature.[71] 243 mg (1 mmol) of compound **1** was dissolved in 5 mL of ethanol and 3 mmol of hydrazine hydrate was added into it. The reaction mixture was refluxed for 6 h, and yellow precipitates were collected after filtration. Precipitates were washed with ethanol (10 mL) three times and dried under vacuum. The yield was 65%. $^1$H NMR (400 MHz, DMSO-$d_6$): $\delta$ 9.46 (s, 1H), 8.93 (s, 1H), 8.74 (d, $J$ = 8.5 Hz, 1H), 8.66 (d, $J$ = 8.4 Hz, 1H), 8.06−7.99 (m, 1H), 5.82 (s, 2H); $^{13}$C NMR (101 MHz, DMSO-$d_6$): $\delta$ 160.60, 159.93, 146.43, 136.96, 134.48, 131.36, 130.33, 129.79, 128.82, 124.26, 123.42, 122.82. HRMS (SI, $m/z$) for $[C_{12}H_7N_3O_4 + H]^+$: calcd, 258.0437; found 258.0495.

**Synthesis of S-13 and S-21.** They were synthesized according to literature reports with little modification.[72] To the ethanolic solution of **1** (243 mg, 1 mmol), respective amine (1.4 mmol) was added and the reaction mixture was refluxed for 18 h. The light yellow-colored precipitates were filtered and washed with ethanol. The obtained precipitates were dried under vacuum to get pure products.

**S-13**: yield 65%. $^1$H NMR (400 MHz, DMSO-$d_6$): $\delta$ 9.49 (d, $J$ = 2.3 Hz, 1H), 8.92 (d, $J$ = 2.4 Hz, 1H), 8.78 (d, $J$ = 8.4 Hz, 1H), 8.64 (d, $J$ = 7.2 Hz, 1H), 8.27 (s, 1H), 8.07−8.03 (m, 2H), 7.78 (d, $J$ = 2.5 Hz, 1H), 7.46−7.42 (m, 1H), 7.02 (d, $J$ = 8.7 Hz, 1H). $^{13}$C NMR (101 MHz, DMSO-$d_6$): $\delta$ 171.83, 163.80, 163.28, 161.72, 146.34, 136.84, 136.15, 134.38, 131.48, 131.21, 130.50, 130.25, 129.76, 126.69, 125.32, 123.84, 123.26, 117.98. HRMS (SI, $m/z$) for $[C_{19}H_{10}N_2O_7 + H]^+$: calcd, 379.0488; found 379.0555.

**S-21**: yield 68%. $^1$H NMR (400 MHz, chloroform-$d$): $\delta$ 9.34 (s, 1H), 9.18 (s, 1H), 8.83 (d, $J$ = 8.2 Hz, 1H), 8.47 (d, $J$ = 8.5 Hz, 1H), 8.01−7.92 (m, 1H), 7.40−7.32 (m, 1H), 7.15−7.07 (m, 1H), 7.02 (d, $J$ = 18.3 Hz, 1H), 6.73 (d, $J$ = 13.9 Hz, 1H). HRMS (SI, $m/z$) for $[C_{18}H_{10}N_2O_5 + H]^+$: calcd, 335.2824; found 335.0591.

**Synthesis of 2.** Compound **2** was synthesized according to the procedure reported in the literature with little modification.[73] In aqueous solution of KOH (2 g in 15 mL water), 1 g of 1,8-naphthalic anhydride was added and stirred at room temperature for 30 min. After 30 min, bromine water was added to the mixture over 3 h dropwise with vigorous stirring and heated at 65 °C for 10 h. After 10 h, concentrated HCl was added to obtain a brown precipitate. The obtained precipitates were further treated with NaOH and filtered. The filtrate was again acidified with HCl to get brown precipitates. The obtained precipitates were dried under vacuum.

**Synthesis of 3.** 400 mg (1.45 mmol) of **2** was dissolved in 2 mL of $H_2SO_4$ at 0 °C. 0.5 mL of $HNO_3$ in 0.5 mL $H_2SO_4$ was added dropwise to the reaction mixture at 0 °C and the reaction mixture was stirred for 5 h at 5 °C. After 6 h, the reaction mixture was poured over ice to get yellow-colored



DOI: 10.1021/acsomega.8b03638
ACS Omega 2019, 4, 5829−5838

precipitates. The obtained precipitates were filtered out and washed with cold acetonitrile. The yellow-colored precipitates were dried under vacuum to get pure a pale yellow-colored compound **3**. Yield: 65%. $^1$H NMR (400 MHz, DMSO-$d_6$): $\delta$ 8.89 (s, 1H), 8.80 (dd, $J$ = 8.6, 1.0 Hz, 1H), 8.71 (dd, $J$ = 7.3, 1.0 Hz, 1H), 8.15 (dd, $J$ = 8.6, 7.3 Hz, 1H).

**Synthesis of 4.** 2 g (6.25 mmol) of compound **3** was dissolved in 2 mL of concentrated hydrochloric acid, and 15 g of tin chloride in 3 mL of hydrochloric acid was added dropwise. After 2 h of reflux, precipitates were filtered off and washed with water and ethanol followed by diethyl ether. The obtained yellow-colored product was dried under vacuum to get compound **4** and used in further reaction without any characterization.

**Synthesis of S-15.** 0.342 mmol (100 mg) of compound **4** was dissolved in 2 mL of absolute ethanol. To the ethanolic solution, 1.56 mmol (50 mg) of hydrazine hydrates was added dropwise and the solution was refluxed for 3 h. After 3 h, the solution was cooled to room temperature and filtered. Yellow-colored precipitates were washed with ethanol and dried under vacuum to get pure compound **S-15**. Yield: 72%. $^1$H NMR (400 MHz, DMSO-$d_6$): $\delta$ 8.21 (d, $J$ = 9.4 Hz, 1H), 8.15 (d, $J$ = 7.3 Hz, 1H), 8.10 (s, 1H), 7.79−7.70 (m, 1H), 6.31 (s, 2H), 5.71 (s, 2H); $^{13}$C NMR (101 MHz, DMSO-$d_6$): $\delta$ 161.03, 160.70, 145.95, 132.14, 130.61, 129.08, 126.50, 122.51, 122.37, 122.24, 120.46, 107.30. HRMS (SI, $m/z$) for $[C_{12}H_8BrN_3O_2 + H]^+$: calcd, 305.9800; found 305.9866.

**Spectroscopic Studies.** All solutions were prepared at room temperature (25 ± 2 °C). The solutions were mixed properly before recording any measurements. The DNA-binding studies of **S-15** were performed in DMSO/$H_2O$ (4:6, v/v) solution. The titration was performed in a volumetric flask and DNA was added stepwise. The fluorescence spectra of **S-15** were recorded with excitation wavelength at 430 nm; the excitation and emission slit width was 10 nm.

**Staining and Fluorescence Imaging.** For cell-imaging studies, a fresh culture of *L. pneumophila* ssp1 was grown on buffered charcoal yeast extract (BCYE) agar medium. Bacterial colonies were transferred into a PBS solution. In order to remove culture medium traces, the prepared bacteria suspension was centrifuged for 30 min at 3000 rpm. This produced a pellet of bacteria at the bottom of an Eppendorf tube with discarder supernatant liquid. The pellet was than suspended in PBS. The concentration of bacteria was determined by optical density (OD) measurements (0.1 $OD_{600nm}$ corresponds to 8 × $10^7$ *L. pneumophila*/mL). For the present study, 4 × $10^5$ CFU/mL concentration of *L. pneumophila* was used. The stock solution of **S-15** (30 $\mu$M) was prepared in DMSO/$H_2O$ (4:6, v/v). Bacteria were incubated with **S-15** for 1 h. It was followed by centrifugation for 30 min at 3000 rpm. The supernatant liquid was removed and the pellet was re-suspended in PBS.

The heat-killed *L. pneumophila* was prepared by incubating a suspension of live *L. pneumophila* at 2 × $10^7$ CFU/mL at 90 °C for 20 min. 4 × $10^5$ heat-killed *Legionella*/mL were than incubated with the **S-15** dye for 1 h. It was followed by centrifugation for 30 min at 3000 rpm. The supernatant liquid was removed and the pellet was re-suspended in PBS. The heat-killed process efficiency was confirmed by growth test on L-cysteine BCYE agar.

**Substrate for *Legionella* Immobilization.** GaAs(001) samples were cleaned in an ultrasonic bath with OptiClear, acetone, and isopropanol sequentially for 5 min each. Following the cleaning steps, the samples were dried under a flow of compressed nitrogen and etched in a solution of $NH_4OH$ (28%) for 2 min at room temperature. Freshly etched GaAs samples were rinsed with deoxygenated anhydrous ethanol and immediately incubated for 20 h at room temperature in a 2 mM mixture of b-PEG (1:15) and HDT (14:15) thiols diluted in deoxygenated anhydrous ethanol. After the thiolation step, the GaAs samples were rinsed with deoxygenated anhydrous ethanol and dried. Following this step, the samples were incubated for 2 h at room temperature in PBS (1×) solution containing 200 $\mu$g/mL of neutravidin. Thereafter, the neutravidin-coated samples were immersed for 1 h at room temperature in a solution of biotinylated polyclonal antibodies against *L. pneumophila* diluted in PBS (1×) at 0.1 mg/mL.

**Cell Counting.** The ImageJ software (NIH free software) was employed for cell counting. Each data set is the average of three independent experiments.

## ■ ASSOCIATED CONTENT

### Supporting Information

The Supporting Information is available free of charge on the ACS Publications website at DOI: 10.1021/acsomega.8b03638.

Full experimental details and characterization of investigated materials (DLS spectra of **S-15** at different concentrations; temperature-dependent absorbance; MTT assay, $^1$H NMR, $^{13}$C NMR spectra, and HRMS spectra) (PDF)

## ■ AUTHOR INFORMATION


### Corresponding Authors

*E-mail: nsingh@iitrpr.ac.in (N.S.).
*E-mail: jan.j.dubowski@usherbrooke.ca (J.J.D.).

### ORCID

Narinder Singh: 0000-0002-8794-8157
Jan J. Dubowski: 0000-0003-0022-527X

### Present Address

§School of Life & Environmental Sciences, Deakin University, Waurn Ponds, Victoria, 3216, Australia.


### Author Contributions

H.S. and J.S. contributed equally. All authors have given approval to the final version of the paper.

### Notes

The authors declare no competing financial interest.

## ■ ACKNOWLEDGMENTS

This research was supported by the joint DBT/IC-IMPACTS research project on *Portable Diagnostics and Analyzers*, the Natural Sciences and Engineering Research Council of Canada (NSERC) STPGP no. 494057, and the Canada Research Chair in Quantum Semiconductors Program (grant no. 950-220304). The help provided by technical staff of the Interdisciplinary Institute for Technological Innovation of the Université de Sherbrooke is greatly appreciated.

## ■ REFERENCES

(1) Maji, B.; Bhattacharya, S. Advances in the molecular design of potential anticancer agents via targeting of human telomeric DNA. *Chem. Commun.* **2014**, *50*, 6422−6438.



DOI: 10.1021/acsomega.8b03638
*ACS Omega* 2019, 4, 5829−5838

(2) Gill, M. R.; Garcia-Lara, J.; Foster, S. J.; Smythe, C.; Battaglia, G.; Thomas, J. A. A ruthenium(II) polypyridyl complex for direct imaging of DNA structure in living cells. *Nat. Chem.* **2009**, *1*, 662−667.
(3) Choi, K. Y.; Liu, G.; Lee, S.; Chen, X. Theranostic nanoplatforms for simultaneous cancer imaging and therapy: current approaches and future perspectives. *Nanoscale* **2012**, *4*, 330−342.
(4) Boer, D. R.; Canals, A.; Coll, M. DNA-binding drugs caught in action: the latest 3D pictures of drug-DNA complexes. *Dalton Trans.* **2009**, 399−414.
(5) Palchaudhuri, R.; Hergenrother, P. J. DNA as a target for anticancer compounds: methods to determine the mode of binding and the mechanism of action. *Curr. Opin. Biotechnol.* **2007**, *18*, 497−503.
(6) Cardin, C. J.; Kelly, J. M.; Quinn, S. J. Photochemically active DNA-intercalating ruthenium and related complexes - insights by combining crystallography and transient spectroscopy. *Chem. Sci.* **2017**, *8*, 4705−4723.
(7) Pages, B. J.; Ang, D. L.; Wright, E. P.; Aldrich-Wright, J. R. Metal complex interactions with DNA. *Dalton Trans.* **2015**, *44*, 3505−3526.
(8) Cao, Q.; Li, Y.; Freisinger, E.; Qin, P. Z.; Sigel, R. K. O.; Mao, Z.-W. G-quadruplex DNA targeted metal complexes acting as potential anticancer drugs. *Inorg. Chem. Front.* **2017**, *4*, 10−32.
(9) Lauria, A.; Bonsignore, R.; Terenzi, A.; Spinello, A.; Giannici, F.; Longo, A.; Almerico, A. M.; Barone, G. Nickel(ii), copper(ii) and zinc(ii) metallo-intercalators: structural details of the DNA-binding by a combined experimental and computational investigation. *Dalton Trans.* **2014**, *43*, 6108−6119.
(10) Granzhan, A.; Kotera, N.; Teulade-Fichou, M.-P. Finding needles in a basestack: recognition of mismatched base pairs in DNA by small molecules. *Chem. Soc. Rev.* **2014**, *43*, 3630−3665.
(11) Martin, R. M.; Leonhardt, H.; Cardoso, M. C. DNA labeling in living cells. *Cytometry, Part A* **2005**, *67*, 45−52.
(12) Zhou, J.; Chang, A.; Wang, L.; Liu, Y.; Liu, X.; Shangguan, D. Effects of side chains on DNA binding, cell permeability, nuclear localization and cytotoxicity of 4-aminonaphthalimides. *Org. Biomol. Chem.* **2014**, *12*, 9207−9215.
(13) Pfeifer, G. P.; You, Y.-H.; Besaratinia, A. Mutations induced by ultraviolet light. *Mutat. Res.* **2005**, *571*, 19−31.
(14) Li, C.; Yu, M.; Sun, Y.; Wu, Y.; Huang, C.; Li, F. A Nonemissive Iridium(III) Complex That Specifically Lights-Up the Nuclei of Living Cells. *J. Am. Chem. Soc.* **2011**, *133*, 11231−11239.
(15) Hayashi, Y.; Obata, N.; Tamaru, M.; Yamaguchi, S.; Matsuo, Y.; Saeki, A.; Seki, S.; Kureishi, Y.; Saito, S.; Yamaguchi, S.; Shinokubo, H. Facile Synthesis of Biphenyl-Fused BODIPY and Its Property. *Org. Lett.* **2012**, *14*, 866−869.
(16) Nunnally, B. K.; He, H.; Li, L.-C.; Tucker, S. A.; McGown, L. B. Characterization of Visible Dyes for Four-Decay Fluorescence Detection in DNA Sequencing. *Anal. Chem.* **1997**, *69*, 2392−2397.
(17) Jia, K.; Wan, Y.; Xia, A.; Li, S.; Gong, F.; Yang, G. Characterization of Photoinduced Isomerization and Intersystem Crossing of the Cyanine Dye Cy3. *J. Phys. Chem. A* **2007**, *111*, 1593−1597.
(18) Wu, X.; Sun, X.; Guo, Z.; Tang, J.; Shen, Y.; James, T. D.; Tian, H.; Zhu, W. In Vivo and in Situ Tracking Cancer Chemotherapy by Highly Photostable NIR Fluorescent Theranostic Prodrug. *J. Am. Chem. Soc.* **2014**, *136*, 3579−3588.
(19) Araneda, J. F.; Piers, W. E.; Heyne, B.; Parvez, M.; McDonald, R. High Stokes Shift Anilido-Pyridine Boron Difluoride Dyes. *Angew. Chem., Int. Ed.* **2011**, *50*, 12214−12217.
(20) Shcherbakova, D. M.; Hink, M. A.; Joosen, L.; Gadella, T. W. J.; Verkhusha, V. V. An Orange Fluorescent Protein with a Large Stokes Shift for Single-Excitation Multicolor FCCS and FRET Imaging. *J. Am. Chem. Soc.* **2012**, *134*, 7913−7923.
(21) Banerjee, S.; Veale, E. B.; Phelan, C. M.; Murphy, S. A.; Tocci, G. M.; Gillespie, L. J.; Frimannsson, D. O.; Kelly, J. M.; Gunnlaugsson, T. Recent advances in the development of 1,8-naphthalimide based DNA targeting binders, anticancer and fluorescent cellular imaging agents. *Chem. Soc. Rev.* **2013**, *42*, 1601−1618.
(22) Braña, M. F.; Cacho, M.; Ramos, A.; Teresa Domínguez, M.; Pozuelo, J. M.; Abradelo, C.; Fernanda Rey-Stolle, M.; Yuste, M.; Carrasco, C.; Bailly, C. Synthesis, biological evaluation and DNA binding properties of novel mono and bisnaphthalimides. *Org. Biomol. Chem.* **2003**, *1*, 648−654.
(23) Braña, M. F.; Cacho, M.; García, M. A.; de Pascual-Teresa, B.; Ramos, A.; Domínguez, M. T.; Pozuelo, J. M.; Abradelo, C.; Rey-Stolle, M. F.; Yuste, M.; Báñez-Coronel, M.; Lacal, J. C. New Analogues of Amonafide and Elinafide, Containing Aromatic Heterocycles: Synthesis, Antitumor Activity, Molecular Modeling, and DNA Binding Properties. *J. Med. Chem.* **2004**, *47*, 1391−1399.
(24) Ingrassia, L.; Lefranc, F.; Kiss, R.; Mijatovic, T. Naphthalimides and Azonafides as Promising Anti-Cancer Agents. *Curr. Med. Chem.* **2009**, *16*, 1192−1213.
(25) Qian, X.; Li, Y.; Xu, Y.; Liu, Y.; Qu, B. Highly-efficient DNA photocleavers with long wavelength absorptions: thio-heterocyclic fused naphthalimides containing aminoalkyl side chains. *Bioorg. Med. Chem. Lett.* **2004**, *14*, 2665−2668.
(26) Li, Y.; Xu, Y.; Qian, X.; Qu, B. Naphthalimide-thiazoles as novel photonucleases: molecular design, synthesis, and evaluation. *Tetrahedron Lett.* **2004**, *45*, 1247−1251.
(27) Ott, I.; Xu, Y.; Liu, J.; Kokoschka, M.; Harlos, M.; Sheldrick, W. S.; Qian, X. Sulfur-substituted naphthalimides as photoactivatable anticancer agents: DNA interaction, fluorescence imaging, and phototoxic effects in cultured tumor cells. *Bioorg. Med. Chem.* **2008**, *16*, 7107−7116.
(28) Yang, Q.; Yang, P.; Qian, X.; Tong, L. Naphthalimide intercalators with chiral amino side chains: Effects of chirality on DNA binding, photodamage and antitumor cytotoxicity. *Bioorg. Med. Chem. Lett.* **2008**, *18*, 6210−6213.
(29) Li, Z.; Yang, Q.; Qian, X. Synthesis, antitumor evaluation and DNA photocleaving activity of novel methylthiazonaphthalimides with aminoalkyl side chains. *Bioorg. Med. Chem. Lett.* **2005**, *15*, 3143−3146.
(30) Chanh, T. C.; Lewis, D. E.; Allan, J. S.; Sogandares-Bernal, F.; Judy, M. M.; Utecht, R. E.; Matthews, J. L. Neutralization of HIV-1 and Inhibition of HIV-1-Induced Syncytia by 1,8-Naphthalimide Photoactive Compound. *AIDS Res. Hum. Retrovir.* **1993**, *9*, 891−896.
(31) Chang, S.-C.; Archer, B. J.; Utecht, R. E.; Lewis, D. E.; Judy, M. M.; Matthews, J. L. 4-alkylamino-3-bromo-N-alkyl-1,8-naphthalimides: new photochemically activatable antiviral compounds. *Bioorg. Med. Chem. Lett.* **1993**, *3*, 555−556.
(32) Chanh, T. C.; Lewis, D. E.; Judy, M. M.; Sogandares-Bernal, F.; Michalek, G. R.; Utecht, R. E.; Skiles, H.; Chang, S.-C.; Matthews, J. L. Inhibition of retrovirus-induced syncytium formation by photoproducts of a brominated 1,8-naphthalimide compound. *Antivir. Res.* **1994**, *25*, 133−146.
(33) Braña, M. F.; Castellano, J. M.; Roldán, C. M.; Santos, A.; Vázquez, D.; Jiménez, A. Synthesis and mode(s) of action of a new series of imide derivatives of 3-nitro-1,8 naphthalic acid. *Cancer Chemother. Pharmacol.* **1980**, *4*, 61−66.
(34) Brana, M.; Ramos, A. Naphthalimides as Anticancer Agents: Synthesis and Biological Activity. *Curr. Med. Chem.: Anti-Cancer Agents* **2001**, *1*, 237−255.
(35) Sharma, H.; Kaur, N.; Singh, N. Imine linked 1,8-naphthalimide: Chromogenic recognition of metal ions, density function theory and cytotoxic activity. *Inorg. Chim. Acta* **2012**, *391*, 83−87.
(36) Andersson, B. S.; Beran, M.; Bakic, M.; Silberman, L. E.; Newman, R. A.; Zwelling, L. A. In Vitro Toxicity and DNA Cleaving Capacity of Benzisoquinolinedione (Nafidimide; NSC 308847) in Human Leukemia. *Cancer Res.* **1987**, *47*, 1040−1044.
(37) Su, G. H.; Sohn, T. A.; Ryu, B.; Kern, S. E. A novel histone deacetylase inhibitor identified by high-throughput transcriptional screening of a compound library. *Cancer Res.* **2000**, *60*, 3137−3142.



DOI: 10.1021/acsomega.8b03638
*ACS Omega* 2019, 4, 5829−5838

(38) Waring, M. J.; González, A.; Jiménez, A.; Vázquez, D. Intercalative binding to DNA of antitumour drugs derived from 3-nitro-1,8-naphthalic acid. *Nucleic Acids Res.* **1979**, *7*, 217−230.
(39) Hsiang, Y. H.; Jiang, J. B.; Liu, L. F. Topoisomerase II-mediated DNA cleavage by amonafide and its structural analogs. *Mol. Pharmacol.* **1989**, *36*, 371−376.
(40) Duke, R. M.; Veale, E. B.; Pfeffer, F. M.; Kruger, P. E.; Gunnlaugsson, T. Colorimetric and fluorescent anion sensors: an overview of recent developments in the use of 1,8-naphthalimide-based chemosensors. *Chem. Soc. Rev.* **2010**, *39*, 3936−3953.
(41) de Silva, A. P.; Gunaratne, H. Q. N.; Habib-Jiwan, J.-L.; McCoy, C. P.; Rice, T. E.; Soumillion, J.-P. New Fluorescent Model Compounds for the Study of Photoinduced Electron Transfer: The Influence of a Molecular Electric Field in the Excited State. *Angew. Chem., Int. Ed. Engl.* **1995**, *34*, 1728−1731.
(42) de Silva, A. P.; Nimal Gunaratne, H. Q.; Gunnlaugsson, T. Fluorescent PET(Photoinduced Electron Transfer) reagents for thiols. *Tetrahedron Lett.* **1998**, *39*, 5077−5080.
(43) Tamanini, E.; Katewa, A.; Sedger, L. M.; Todd, M. H.; Watkinson, M. A Synthetically Simple, Click-Generated Cyclam-Based Zinc(II) Sensor. *Inorg. Chem.* **2009**, *48*, 319−324.
(44) Tamanini, E.; Flavin, K.; Motevalli, M.; Piperno, S.; Gheber, L. A.; Todd, M. H.; Watkinson, M. Cyclam-Based "Clickates": Homogeneous and Heterogeneous Fluorescent Sensors for Zn(II). *Inorg. Chem.* **2010**, *49*, 3789−3800.
(45) Pfeffer, F. M.; Buschgens, A. M.; Barnett, N. W.; Gunnlaugsson, T.; Kruger, P. E. 4-Amino-1,8-naphthalimide-based anion receptors: Employing the naphthalimide N-H moiety in the cooperative binding of dihydrogenphosphate. *Tetrahedron Lett.* **2005**, *46*, 6579−6584.
(46) Pfeffer, F. M.; Seter, M.; Lewcenko, N.; Barnett, N. W. Fluorescent anion sensors based on 4-amino-1,8-naphthalimide that employ the 4-amino N-H. *Tetrahedron Lett.* **2006**, *47*, 5241−5245.
(47) Li, Y.; Cao, L.; Tian, H. Fluoride Ion-Triggered Dual Fluorescence Switch Based on Naphthalimides Winged Zinc Porphyrin. *J. Org. Chem.* **2006**, *71*, 8279−8282.
(48) Ryan, G. J.; Quinn, S.; Gunnlaugsson, T. Highly Effective DNA Photocleavage by Novel "Rigid" Ru(bpy)3-4-nitro- and -4-amino-1,8-naphthalimide Conjugates. *Inorg. Chem.* **2008**, *47*, 401−403.
(49) Xu, Z.; Baek, K.-H.; Kim, H. N.; Cui, J.; Qian, X.; Spring, D. R.; Shin, I.; Yoon, J. Zn2+-Triggered Amide Tautomerization Produces a Highly Zn2+-Selective, Cell-Permeable, and Ratiometric Fluorescent Sensor. *J. Am. Chem. Soc.* **2010**, *132*, 601−610.
(50) Xu, Z.; Yoon, J.; Spring, D. R. A selective and ratiometric Cu2+ fluorescent probe based on naphthalimide excimer-monomer switching. *Chem. Commun.* **2010**, *46*, 2563−2565.
(51) Wang, D.; Zhang, X.; He, C.; Duan, C. Aminonaphthalimide-based imidazolium podands for turn-on fluorescence sensing of nucleoside polyphosphates. *Org. Biomol. Chem.* **2010**, *8*, 2923−2925.
(52) Banerjee, S.; Kitchen, J. A.; Gunnlaugsson, T.; Kelly, J. M. Synthesis and photophysical evaluation of a pyridinium 4-amino-1,8-naphthalimide derivative that upon intercalation displays preference for AT-rich double-stranded DNA. *Org. Biomol. Chem.* **2012**, *10*, 3033−3043.
(53) Zeng, Q.; Li, Z.; Dong, Y.; Di, C. a.; Qin, A.; Hong, Y.; Ji, L.; Zhu, Z.; Jim, C. K. W.; Yu, G.; Li, Q.; Li, Z.; Liu, Y.; Qin, J.; Tang, B. Z. Fluorescence enhancements of benzene-cored luminophors by restricted intramolecular rotations: AIE and AIEE effects. *Chem. Commun.* **2007**, 70−72.
(54) Kim, T. H.; Kim, S. H.; Tan, L. V.; Seo, Y. J.; Park, S. Y.; Kim, H.; Kim, J. S. Transition metal ion selective ortho-ester diazophenylcalix[4]arene. *Talanta* **2007**, *71*, 1294−1297.
(55) Yuan, D.; Brown, R. G. Enhanced Nonradiative Decay in Aqueous Solutions of Aminonaphthalimide Derivatives via Water-Cluster Formation. *J. Phys. Chem. A* **1997**, *101*, 3461−3466.
(56) Banerjee, S.; Kitchen, J. A.; Gunnlaugsson, T.; Kelly, J. M. Synthesis and photophysical evaluation of a pyridinium 4-amino-1,8-naphthalimide derivative that upon intercalation displays preference for AT-rich double-stranded DNA. *Org. Biomol. Chem.* **2012**, *10*, 3033−3043.
(57) Saha, S.; Samanta, A. Influence of the Structure of the Amino Group and Polarity of the Medium on the Photophysical Behavior of 4-Amino-1,8-naphthalimide Derivatives. *J. Phys. Chem. A* **2002**, *106*, 4763−4771.
(58) Ryan, G. J.; Poynton, F. E.; Elmes, R. B. P.; Erby, M.; Williams, D. C.; Quinn, S. J.; Gunnlaugsson, T. Unexpected DNA binding properties with correlated downstream biological applications in mono vs. bis-1,8-naphthalimide Ru(ii)-polypyridyl conjugates. *Dalton Trans.* **2015**, *44*, 16332−16344.
(59) Kumar, C. V.; Asuncion, E. H. DNA binding studies and site selective fluorescence sensitization of an anthryl probe. *J. Am. Chem. Soc.* **1993**, *115*, 8547−8553.
(60) Rogers, J. E.; Weiss, S. J.; Kelly, L. A. Photoprocesses of Naphthalene Imide and Diimide Derivatives in Aqueous Solutions of DNA. *J. Am. Chem. Soc.* **2000**, *122*, 427−436.
(61) Williams, A. K.; Dasilva, S. C.; Bhatta, A.; Rawal, B.; Liu, M.; Korobkova, E. A. Determination of the drug-DNA binding modes using fluorescence-based assays. *Anal. Biochem.* **2012**, *422*, 66−73.
(62) Ahmadi, F.; Jamali, N.; Jahangard-Yekta, S.; Jafari, B.; Nouri, S.; Najafi, F.; Rahimi-Nasrabadi, M. The experimental and theoretical QM/MM study of interaction of chloridazon herbicide with ds-DNA. *Spectrochim. Acta, Part A* **2011**, *79*, 1004−1012.
(63) Ahmadi, F.; Bakhshandeh, F. In Vitro Study of Damaging Effects of 2,4-Dichlorophenoxyacetic Acid on DNA Structure by Spectroscopic and Voltammetric Techniques. *DNA Cell Biol.* **2009**, *28*, 527−533.
(64) Muslu, H.; Golcu, A.; Tumer, M.; Ozsoz, M. Electrochemical investigation and DNA-binding studies of pefloxacin-metal(II/III) complexes. *J. Coord. Chem.* **2011**, *64*, 3393−3407.
(65) Verma, M.; Kaur, N.; Singh, N. Naphthalimide-Based DNA-Coupled Hybrid Assembly for Sensing Dipicolinic Acid: A Biomarker for Bacillus anthracis Spores. *Langmuir* **2018**, *34*, 6591−6600.
(66) Arjmand, F.; Yousuf, I.; Hadda, T. b.; Toupet, L. Synthesis, crystal structure and antiproliferative activity of Cu(II) nalidixic acid-DACH conjugate: Comparative in vitro DNA/RNA binding profile, cleavage activity and molecular docking studies. *Eur. J. Med. Chem.* **2014**, *81*, 76−88.
(67) Nazemi, E.; Aithal, S.; Hassen, W. M.; Frost, E. H.; Dubowski, J. J. GaAs/AlGaAs heterostructure based photonic biosensor for rapid detection of Escherichia coli in phosphate buffered saline solution. *Sens. Actuators, B* **2015**, *207*, 556−562.
(68) Nazemi, E.; Hassen, W. M.; Frost, E. H.; Dubowski, J. J. Monitoring growth and antibiotic susceptibility of Escherichia coli with photoluminescence of GaAs/AlGaAs quantum well microstructures. *Biosens. Bioelectron.* **2017**, *93*, 234−240.
(69) Aziziyan, M. R.; Hassen, W. M.; Morris, D.; Frost, E. H.; Dubowski, J. J. Photonic biosensor based on photocorrosion of GaAs/AlGaAs quantum heterostructures for detection of *Legionella pneumophila*. *Biointerphases* **2016**, *11*, 019301.
(70) Russell, A. D. Lethal effects of heat on bacterial physiology and structure. *Sci. Prog.* **2003**, *86*, 115−137.
(71) Sidhu, J. S.; Singh, A.; Garg, N.; Singh, N. Carbon Dot Based, Naphthalimide Coupled FRET Pair for Highly Selective Ratiometric Detection of Thioredoxin Reductase and Cancer Screening. *ACS Appl. Mater. Interfaces* **2017**, *9*, 25847−25856.
(72) MacGregor, K. A.; Robertson, M. J.; Young, K. A.; von Kleist, L.; Stahlschmidt, W.; Whiting, A.; Chau, N.; Robinson, P. J.; Haucke, V.; McCluskey, A. Development of 1,8-Naphthalimides as Clathrin Inhibitors. *J. Med. Chem.* **2014**, *57*, 131−143.
(73) Verma, M.; Luxami, V.; Paul, K. Synthesis, in vitro evaluation and molecular modelling of naphthalimide analogue as anticancer agents. *Eur. J. Med. Chem.* **2013**, *68*, 352−360.



DOI: 10.1021/acsomega.8b03638
*ACS Omega* 2019, 4, 5829−5838